Search for Dark Matter Candidates Produced in $Z(\ell\ell) + E_T^{\text{miss}}$ Events in 13 TeV Proton-Proton Collisions with the ATLAS Detector at the Large Hadron Collider

by

Kayla McLean
B.Sc., University of Victoria, 2014

A Proposal Submitted in Partial Fulfillment of the
Requirements for the Candidacy of

DOCTOR OF PHILOSOPHY

in the Department of Physics and Astronomy

University of Victoria

Contents

Chapter 1

Introduction

The Standard Model (SM) of particle physics is the most complete theory that exists to describe elementary particles and their interactions. However there are known weaknesses in the SM, one of which is the failure to include a description of dark matter (DM). There is strong evidence from astronomical observations that there is a large excess of matter in the universe that appears to have only gravitational interactions with SM particles. Some examples for the evidence of dark matter include measurements of rotation velocities of spiral galaxies, gravitational lensing effects, and anisotropies in the cosmic microwave background. The standard model of cosmology predicts that dark matter accounts for approximately 27% of the total mass energy of the universe. Although there are many theories to describe possible dark matter candidates, the one of interest here is the WIMP (weakly interacting massive particle). The WIMP is a Dirac fermion, often denoted χ, and is predicted to interact gravitationally and through other force(s), potentially beyond the SM. It is predicted to have a mass between 10 GeV and a few TeV, and have a self-annihilation cross section similar to that of SM weak interactions.

There are three categories of experiments that have potential to observe dark matter: direct detection, indirect detection, and collider production. Figure 1.1 shows a schematic that illustrates their complementarity to one another. Direct detection (DD) experiments attempt to observe recoils in SM particles from scattering with dark matter. Indirect detection (ID) experiments measure decay products from DM annihilation. Collider experiments look for dark matter that is is produced from the annihilation of SM particles. This work focuses on the production of dark matter at the Large Hadron Collider (LHC) using data collected from proton-proton (pp) collisions inside the ATLAS detector.

If it is possible to produce dark matter in collisions of SM particles, then an additional complication is how the presence of dark matter can be determined in a very dense envi-

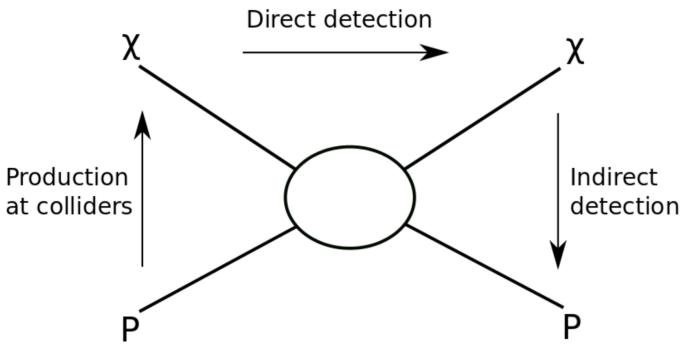

Figure 1.1: Schematic of potential dark matter interactions and their experimental categories.

ronment of high energy particles. Collider experiments use a quantity known as missing transverse momentum, or missing transverse energy, commonly denoted $E_{\mathrm{T}}^{\mathrm{miss}}$, to quantify the amount of invisible decay products in collisions. The plane perpendicular to the beam axis, also known as the transverse plane, is of particular importance in collider experiments. Before colliding, the protons in the beam only move along the beam axis, so the net momentum in the transverse plane is zero. From conservation of momentum, the net transverse momentum after the collision therefore must also be zero. If the transverse momenta of all visible particles produced in the collision are added together vectorially, they should add to zero. But, if invisible particles are present, such as neutrinos or dark matter, then the sum will instead add to a non-zero transverse momentum vector. We therefore infer that there are non-interacting particles produced, and they have a net $E_{\mathrm{T}}^{\mathrm{miss}}$ vector that is the negative of the vectorial sum of the transverse momenta of the visible particles. Hence a dark matter signal would manifest as an excess of collision events with a significant amount of $E_{\mathrm{T}}^{\mathrm{miss}}$ compared to the SM prediction.

In order to pick out events with a large amount of $E_{\mathrm{T}}^{\mathrm{miss}}$, another (visible) particle must be used as a 'tag.' If the amount of missing energy in an event is large, the tag particle will experience a significant amount of recoil against the $E_{\mathrm{T}}^{\mathrm{miss}}$ vector. This gives a mean of identifying potentially interesting events. In this work the Z boson is used as a tag, which is identified in events from a pair of same sign, opposite charge leptons (e^+e^- or $\mu^+\mu^-$). This analysis attempts to find dark matter with $Z(\ell\ell) + E_T^{\mathrm{miss}}$ events, and is therefore commonly referred to as the mono-$Z(\ell\ell)$ search. Other mono-X searches use different SM particles as tags, such as a jet, photon, H, or W.

The ATLAS experiment has been in a period of intense data-taking since the start of Run 2 in 2015, with pp collisions at a centre-of-mass energy of 13 TeV. As data continues to

be collected until the end of 2018, the discovery potential for dark matter at the LHC has never been higher. This document summarizes the work done on the mono-$Z(\ell\ell)$ analysis so far as well as the prospects for the full Run 2 dataset. Chapter 2 includes a summary of the dark matter models considered in the analysis, as well as a brief description of the LHC and the ATLAS detector. Chapter 3 covers the details of the search with a focus on the work done for the results obtained using the 2015 and 2015+2016 datasets. Chapter 4 describes the plan to analyze the complete Run 2 dataset over the full period from 2015-2018.

Chapter 2

Dark Matter Searches with the ATLAS Detector

2.1 Dark Matter Theory

2.1.1 Effective Field Theories

Effective field theories (EFTs) were the primary models studied in $E_T^{\text{miss}} + X$ dark matter searches in Run 1, when the centre-of-mass energy was 8 TeV. In short, these theories assume that a dark matter pair is produced by means of a contact interaction with a quark and antiquark, as illustrated in Figure 2.1. These types of models offer a straightforward means to compare collider results to DD or ID experiments. However, an important caveat of EFTs is that they are only valid when the mass of the mediating particle between the $\chi\bar{\chi}$ and $q\bar{q}$ is much heavier than the momentum transfer of the process. Now that the centre-of-mass energy has increased to 13 TeV in Run 2, these EFTs are no longer valid. Thus, a new baseline model is used in Run 2 with the mediator particle explicitly included.

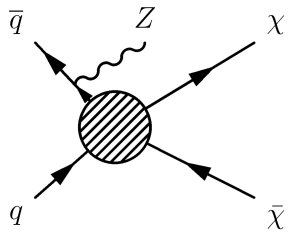

Figure 2.1: An example EFT with a $Z + \chi\bar{\chi}$ final state with a Z emitted as ISR.

2.1.2 Simplified Models

Leading order simplified models are the benchmark models used for $E_T^{\text{miss}} + X$ searches in Run 2. An example s-channel diagram for the $Z + E_T^{\text{miss}}$ signal is shown in Figure 2.2. These models are considered 'simplified' because they introduce the minimum number of parameters needed to include a mediator between SM and dark matter particles (compared to more complicated models such as supersymmetry).

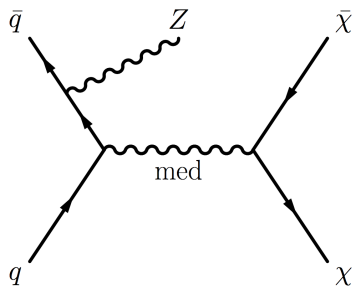

Figure 2.2: s-channel diagram for WIMP pair production with a Z emitted as ISR.

Simplified models introduce five BSM parameters: the mass of the WIMP, m_χ, the mass of the mediating particle, m_{med}, the couplings of the mediator to the SM (to dark matter), g_q (g_χ), and the width of the mediator Γ_{med}. The mediator particle can be spin-0 (scalar or pseudo-scalar) or spin-1 (vector or axial-vector).

Following the recommendations of TODO, for spin-0 models the couplings are set to $g_q = g_\chi = 1.0$. The Yukawa couplings y_i^f are also included that are proportional to the quark masses. For spin-1 models the couplings are fixed to $g_q = 0.25$ and $g_\chi = 1.0$. In addition, assuming that the mediator has no additional decay modes, Γ_{med} is set to the so-called minimal width, which is fixed by g_q, g_χ, m_χ, and m_{med}. The couplings were chosen to correspond with a rough estimate of the lower sensitivity of the mono-jet analysis in Run 2, and so that $\Gamma_{\text{med}}/m_{\text{med}} <\sim 0.05$.

Run 2 analyses have adopted the s-channel exchange of an axial-vector mediator as the primary benchmark scenario. This choice is motivated by the findings in TODO that show that collider searches can be more sensitive than DD experiments at low values of m_χ for this type of mediator.

Although they have advantages compared to EFTs, simplified models are not a complete theory, and violate unitarity for some regions of parameter space. In Run 2 they have been and will continue to be exceedingly useful in providing a guideline for the ATLAS and CMS collaborations to follow in tandem, but there is now a push towards studying more theoretically complete models.

2.1.3 2HDM+PS Model

A model that is becoming popular in mono-X dark matter searches is known as the two Higgs doublet + pseudo-scalar (2HDM+PS) model [1]. 2HDMs are essential for many well-motivated BSM theories. They are perturbative and avoid violating unitarity by allowing mixing between the dark matter mediator and other bosons.

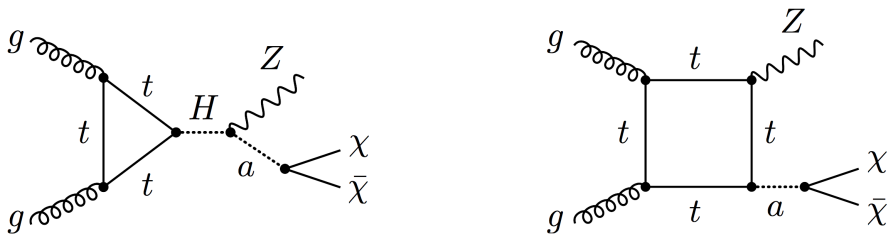

Figure 2.3: Representative diagrams of the mono-Z signature in the 2HDM+PS model. The second diagram can have $a \to A$.

Figure 3.7 shows the two main diagrams of the 2HDM+PS model with the mono-Z signature. This model introduces two CP-even scalars H and h (where h is the SM Higgs), one CP-odd pseudo-scalar A, two charged scalars H^+ and H^-, and the pseudo-scalar a that couples the SM particles to dark matter. There are also the parameters $\sin(\theta)$ and $\tan(\beta)$.

TODO - mono-Z enhancement

2.2 The LHC and the ATLAS Detector

The Large Hadron Collider (LHC) is the world's largest particle accelerator with a circumference of 27 km. Superconducting magnets are used to accelerate two beams of protons up to nearly the speed of light. The beams are then brought to collision at various points around the LHC. Located at one of these collision points is the ATLAS detector, one of the two multipurpose detectors at the LHC. The LHC has been colliding protons at a centre-of-mass (COM) energy of 13 TeV since 2015. During this time ATLAS has been continuously taking data.

The amount of pp collision data delivered by the LHC is quantified by the *luminosity*. The total number of pp collisions N detected over all time t is related to the cross section for pp collisions σ, and can be expressed in terms of either the instantaneous luminosity L or the integrated luminosity $\mathcal{L}$:

$$N = \sigma = \int L \mathrm{d}t = \sigma\mathcal{L} \tag{2.1}$$

$\mathcal{L}$ is the measure of total data collected that is frequently quoted in ATLAS. It has units of cm^2, but a more frequently used unit is the inverse barn. 1 b = 10^{-28} m^2. The total amount of data delivered by the LHC since 2015 is currently 93 fb^{-1} from 2015-2017. ATLAS has recorded a total of 86 fb^{-1}, with 80 fb^{-1} that is good for physics analyses.

An overview of the ATLAS detector is shown in Figure 2.4. It is composed of four major subsystems. The innermost system is the inner detector (ID) which measures the tracks of charged particles very near to the collision point. It consists of three layers known as the pixel detector, semiconductor tracker (SCT), and transition radiation tracker (TRT). The innermost pixel detector has the highest resolution granularity in the detector and consists of 80 million pixels. The SCT consists of 60 m^2 of silicon microstrips with densely packed readout channels, and the TRT consists of 300,000 straw tubes with wires inside to measure tracks from ionization. The ID is encased in a solenoid magnet that exerts a 2 Tesla magnetic field. The magnetic field causes the paths of charged particles to bend. The momentum of the particles can be determined from the curvature of the tracks.

Moving outward from the centre of the detector, the next subsystems are the electromagnetic (EM) and hadronic (HAD) calorimeters. The EM system is entirely composed of liquid argon (LAr) calorimetery, while the HAD system includes the tile calorimeter in the barrel region and LAr calorimetery in the end caps. The calorimeters are dense and designed to stop particles completely so that their energy is deposited entirely inside the detector. The EM calorimeter is designed to stop particles that interact electromagnetically (electrons and

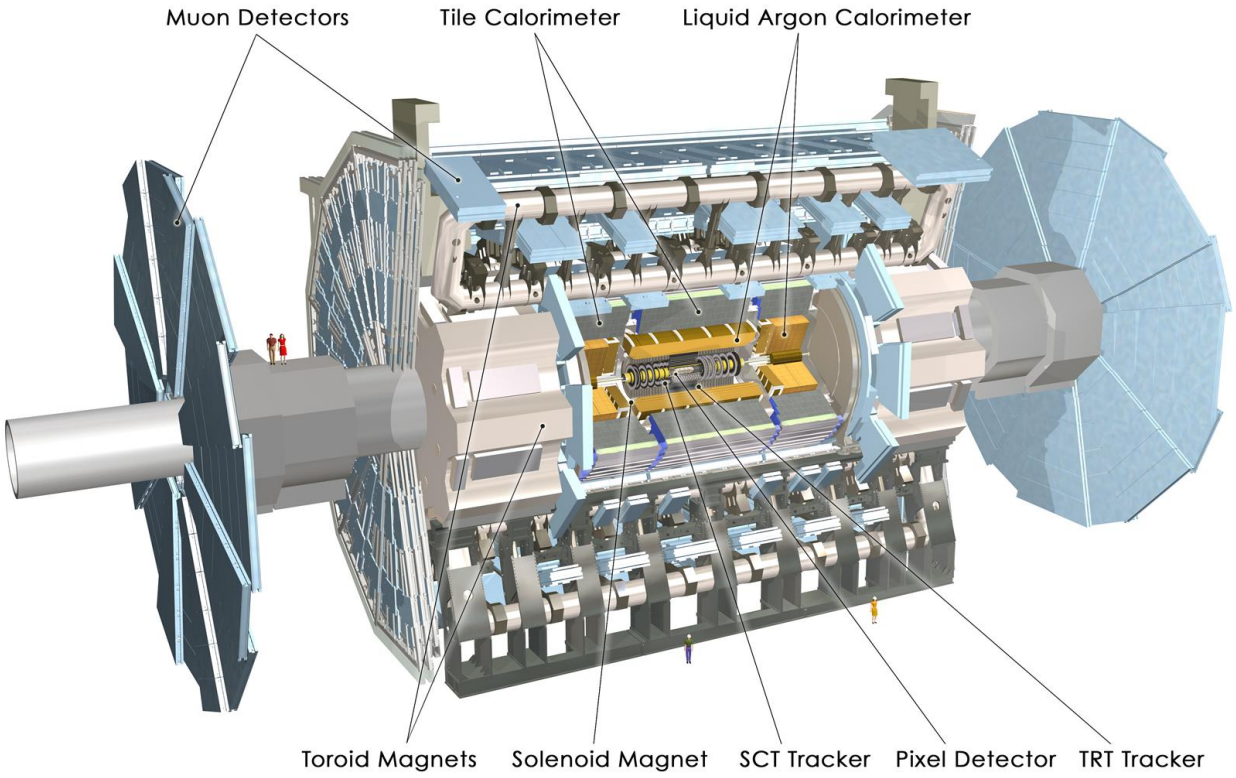

Figure 2.4: The ATLAS detector.

photons) while the HAD calorimeter is designed to stop hadrons (e.g. protons and neutrons). The LAr calorimeter consists of alternating layers of copper absorber material and LAr ionization chambers, while the tile calorimeter alternates between layers of steel and plastic scintillators.

The outermost and largest system of the detector is the muon spectrometer (MS). Muons will interact minimally with the detector and so the MS is designed to measure their momenta from tracks. The MS consists of several systems. Monitored drift tubes (MDTs) are used in the barrel and end caps for measuring track curvature. Resistive plate chambers (RPCs), cathode strip chambers (CSCs), and thin gap chambers (TGCs) are used for precision coordinate measurements throughout the spectrometer. The MS also contains the ATLAS toroid magnet system.

Events that occur in the detector are recorded by the ATLAS trigger system, consisting of tiers that act at the hardware and software levels. The trigger makes decisions on which events to record to disk or not based on energy deposits, etc.

Chapter 3

The Mono-$Z(\ell\ell)$ Search

This chapter summarizes the previous work done. Section 3.1 gives an overview of the analysis, while Sections 3.2 - 3.5 discuss specific contributions in more detail.

3.1 Analysis Overview

There are several important aspects of the mono-Z search. The analysis has been repeated fully twice during Run 2, once with the 2015 dataset (3.2 fb^{-1}) and again with the 2015+2016 dataset (36.1 fb^{-1}). The next result will not be ready until the full 2015-2018 Run 2 dataset is collected. The techniques discussed in this section are mainly based on the previous results from the 2015+2016 dataset.

One of the the first steps of the analysis is to optimize the event selection for the specific signal being considered in the search. A *signal region* must be chosen using some metric that optimizes the amount of signal compared to background. Background events are caused by SM processes that produce the same signature as the dark matter signal. Ideally such processes should be as suppressed as possible in the signal region. Event selections are optimized using Monte Carlo (MC) simulated events for signal and backgrounds. ATLAS MC are sophisticated and include effects from the detector, such as energy resolution. In general, events are selected in order to isolate a e^+e^- or $\mu^+\mu^-$ pair that have an invariant mass close to the Z and are recoiling against a sizeable $E_{\mathrm{T}}^{\mathrm{miss}}$ vector. The most important kinematic variables are identified and calculated using reconstructed objects as measured in the ATLAS detector (approximate in MC). Additional selection requirements are used to reduce background contributions while attempting to preserve signal. Two signal regions are used in the mono-Z analysis, one where e^+e^- events are selected and the other where $\mu^+\mu^-$

events are selected.

Another crucial part of the analysis is in-situ background estimation. Once a signal region has been defined, data can then be used to estimate the dominant backgrounds in that region. When possible it is always preferable to use data instead of MC estimations. This is typically done by defining a control region that has a very high purity in background events, and then somehow transferring the estimate into the signal region. The major backgrounds in the analysis are described below with their percent contribution from the 2015+2016 result. They all emulate the signal by producing $\ell\ell + E_T^{\text{miss}}$. All backgrounds except for the ZZ background are estimated from data.

1. $ZZ \to \ell\ell\nu\nu$ (56%): Dominant, irreducible background. Estimated entirely with MC.
2. $WZ \to \ell\nu\ell\ell$ (27%): Lepton from the W is not reconstructed.
3. Z+jets (8%): Jet(s) are mis-measured as fake $E_{\text{T}}^{\text{miss}}$.
4. WW, Wt, $t\bar{t}$, and $Z \to \tau\tau$ (8%): Lepton pair does not come from a Z.
5. W+jets ($< 1\%$): Lepton is misidentified from a jet.

The data-driven estimation techniques for each of the backgrounds are complex and are not discussed in detail here. Previous work on the estimation of the Z+jets background is discussed ahead.

There are several sources of systematic errors that must be considered in any ATLAS analysis. Experimental systematics come from detector effects, such as the uncertainty in identifying an electron, energy uncertainties due to resolution effects, etc. These systematics are applied to MC samples. Data-driven background estimates will have systematic errors associated with the specific estimation technique. These types of systematics are often the dominant source of systematic uncertainties. Finally, there are theoretical systematics associated with the simulated dark matter signal, including errors from QCD, PDF, and parton showering effects. These will be discussed in more detail in the following section.

After defining a signal region, estimating backgrounds in that signal region, and accounting for the systematic uncertainties of the analysis, the signal region is *unblinded* and the agreement between observed data and expected background estimates is quantified. In the mono-Z analysis the $E_{\text{T}}^{\text{miss}}$ is the distribution of interest, where a dark matter signal could manifest. The signal region $E_{\text{T}}^{\text{miss}}$ distributions from the 2015+2016 analysis are shown in Figure 3.1. If an excess in data is found then there is potential for a discovery. However, as in past iterations of the analysis, if no excess is seen then limits can be set on the dark matter model being studied. This is discussed in detail in the final section of this chapter.

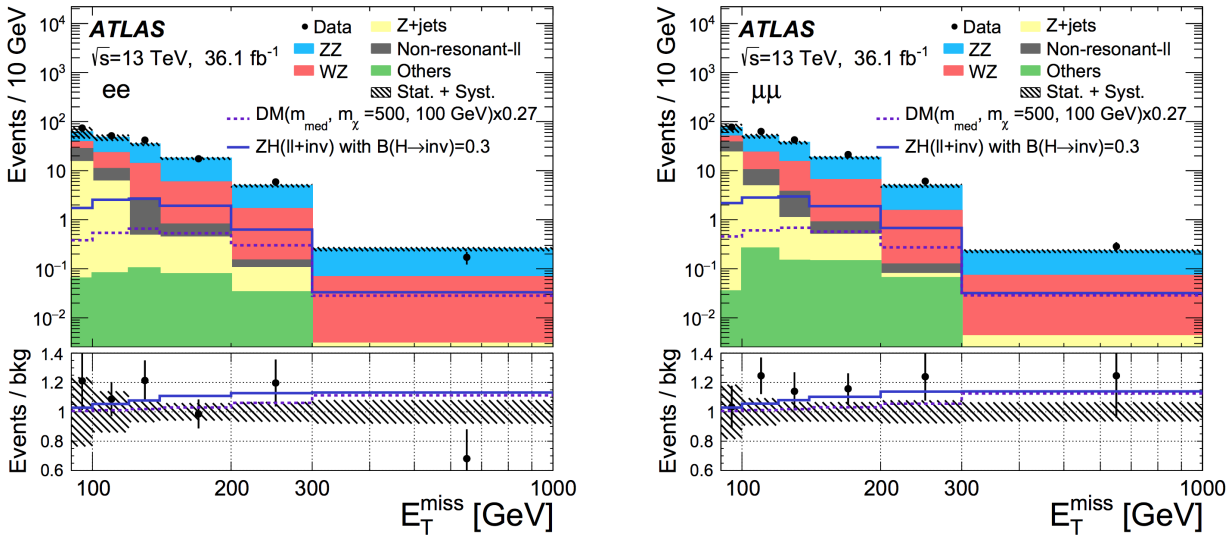

Figure 3.1: Text

3.2 Truth Studies

Truth studies are often useful when we want to ignore the effects of the ATLAS detector. *Reconstructed* MC samples include simulation of the detector, whereas *truth-level* MC samples come directly from the MC generator, typically MadGraph. Studying these samples allow us to study theoretical effects on the signal. In addition, such samples can be produced quickly and locally, whereas reconstructed samples must undergo heavy duty ATLAS reconstruction which can be computationally intensive.

A framework has been adapted, called MonoZTruthUVic, for applying truth-equivalent analysis cuts to truth samples. This allows for the analysis to be reproduced at the truth-level. This is useful for several reasons and allows us to estimate how many signal events are theoretically predicted to be in the signal region.

An important study that must be performed at the truth-level is the estimation of theoretical uncertainties on the signal *acceptance*, the number of signal events that end up in the signal regio. There are potentially significant sources of systematic uncertainties from theory that must be considered. It should be noted that systematics from uncertainties in the parton distribution function (PDF) are evaluated in the analysis but are not discussed in detail here.

The signal acceptance depends on two scales from quantum chromodynamics (QCD) known as the renormalization and factorization scales, μ_r and μ_f. Both scales are arbitrary and arise from finite order perturbation theory. μ_r is related to the renormalization of

ultraviolet divergences, and μ_f qualitatively corresponds to the resolution at which the proton is being probed. The cross section for some hard process depends on these scales via

$$\sigma = \int \mathrm{d}x_1 \mathrm{d}x_2 f_1(x_1, \mu_f^2) f_2(x_2, \mu_f^2) \hat{\sigma}(x_1 p_1, x_2 p_2, \alpha_s(\mu_r), Q^2, \mu_r^2, \mu_f^2), \tag{3.1}$$

where partons 1 and 2 have PDFs f_1 and f_2 and momentum fractions $x_1 p_1$ and $x_2 p_2$ respectively. Q is the scale of the hard scatter process determined by the cross section $\hat{\sigma}$. In short, by simulating dark matter MC with different values for μ_f and μ_r and then applying truth-level analysis cuts, the systematic error on the acceptance due to the choice of scales can be quantified. The convention is to generate two variational samples with $\mu_r = \mu_f$, where the scales are doubled in one sample and halved in the other. Then the signal acceptance for both variational samples is calculated and compared to the nominal acceptance. The largest change is taken as the systematic error. This systematic has been observed to be independent of m_{DM}, so the errors are evaluated as a function of m_{med}. An example of the errors previously used for axial-vector signals is illustrated in Figure 3.2. These errors are on the order of 1-2%.

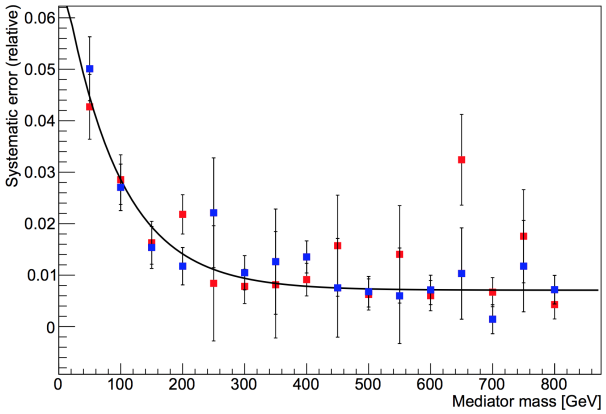

Figure 3.2: QCD scale uncertainties as a function of mediator mass for axial-vector signals. Red and blue points correspond to errors obtained from the ee and $\mu\mu$ signal regions respectively.

The other source of theoretical uncertainty on the signal acceptance comes from parton showering effects. In the MC samples used by ATLAS, after the hard scatter is simulated it is run through a showering simulator called Pythia. Pythia adds in several physical effects such as the underlying event (UE), initial and final state radiation (ISR and FSR) of extra jets, and multiple parton interactions (MPI). These are complicated processes governed by QCD and the number of parameters in Pythia that can be set are extensive. To simplify

this, ATLAS has a standardized PYTHIA *tune*, i.e. a set of parameters that serve as the default to be used in MC showering. The signal acceptance depends on the choice of this tune. The uncertainty is evaluated using a prescription whereby ten variations are used to account for each general effect. As for the QCD scale uncertainties, variational MC samples are produced according to each variation, and the difference in the signal acceptance is evaluated compared to the nominal showering. These systematics are typically on the order of 5%.

3.3 Estimation of the Z+jets Background

3.3.1 ABCD Method

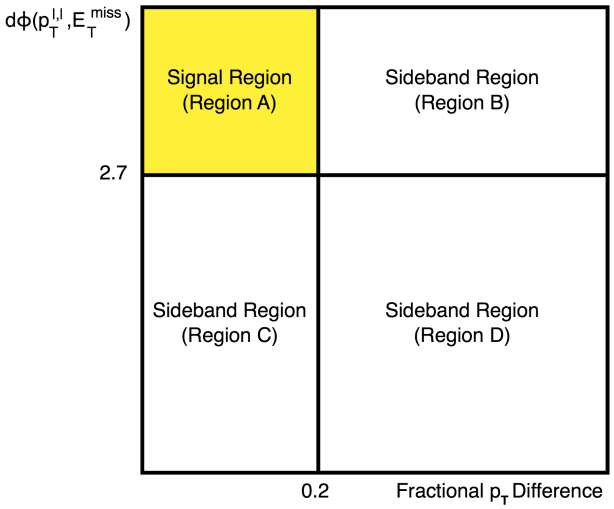

Figure 3.3: Scheme of the ABCD method.

One data-driven technique for estimating the Z+jets background is the ABCD method. This was the primary estimation method used for the 2015 result. A schematic of the method is shown in Figure 3.3. Four regions are defined using two of the kinematic variables from the event selection. This pair of variables is chosen to optimize event statistics in the sideband regions (B, C, and D) and to minimize the correlation between them. Region A is the signal region, the target region that we are trying to estimate the background in. The number of background events in the sidebands are used to estimate the number of background events in A using the assumption that $N_A/N_C = N_B/N_D$. This is true if there is no correlation between the two variables. Then the number of Z+jets events in A is given by:

$$N_{\mathrm{A}}^{\mathrm{est}} = N_{\mathrm{C}}^{\mathrm{obs,corr}} \times \frac{N_{\mathrm{B}}^{\mathrm{obs,corr}}}{N_{\mathrm{D}}^{\mathrm{obs,corr}}} \tag{3.2}$$

N_{B}, N_{C}, and N_{D} are the observed number of events in each sideband control region with non-Z+jets events subtracted (using MC).

The main challenges for this method come from having correlations between the two variables and having enough statistics in data in all of the sidebands. The validity of this technique is evaluated by looking at the agreement between the three ratios $N_{\mathrm{A}}/N_{\mathrm{C}}$ (MC), $N_{\mathrm{B}}/N_{\mathrm{D}}$ (MC), and $N_{\mathrm{B}}/N_{\mathrm{D}}$ (data). If the method works perfectly then these ratios will agree. In addition, the agreement of these ratios should agree as the other event selections are applied. However, correlations cause deviations in the agreement, and low statistics in one or more of the sidebands can lead to large errors on the ratios after all selections are applied. And, if the ratios change with other selections, this suggests more complicated correlations with other variables that enhance the correlation between the two variables used for the method. These effects are all taken into account with systematic errors that are evaluated to be about $\pm 70\%$ on the Z+jets estimate. These turned out to be dominant uncertainties in the analysis for the 2015 result.

3.3.2 γ+jets Technique

The Z+jets estimation had to be modified for the 2015+2016 result. The event selection was reoptimized and introduced new variables, and correlations had a more pronounced effect in the ABCD method. Because of this, a second technique was developed alongside a modified ABCD method. The technique is known as the γ+jets reweighting method. The theory is described in [2] and the application has been adapted from an ATLAS SUSY search [3].

The γ+jets method uses events with a photon and jets to estimate the fake $E_{\mathrm{T}}^{\mathrm{miss}}$ in Z+jets events. γ+jets event topologies are similar to Z+jets events as they both consist of a well-measured Z or photon recoiling against jets, and the $E_{\mathrm{T}}^{\mathrm{miss}}$ arises from jet mismeasurements. However there are some kinematic differences that need to be accounted for. This is done by reweighting the γ+jets MC events to transport them to Z+jets MC events. Typically the p_{T} distribution of the photon is scaled to match the p_{T} distribution of the Z (i.e. the p_{T} of the two leptons). The multiplicative factor needed to scale each p_{T} bin is used as an event weight for the γ+jets events:

$$w(p_{\mathrm{T}}^{\gamma}) = \frac{N_{Z+\mathrm{jets}}(p_{\mathrm{T}}^{\ell\ell})}{N_{\gamma+\mathrm{jets}}(p_{\mathrm{T}}^{\gamma})} \tag{3.3}$$

After the reweighting the $E_{\mathrm{T}}^{\mathrm{miss}}$ distribution for the γ+jets events improves to match the Z+jets events (most obviously the tail increases at high $E_{\mathrm{T}}^{\mathrm{miss}}$). The reweighting is applied fairly early in the event selection and then subsequent selections are applied; the agreement between γ+jets and Z+jets events is monitored down to the signal region. Once reliable agreement is seen, then the method can be performed using data instead of MC.

In the mono-Z analysis, p_{T} reweighting was not sufficient to have good agreement between γ+jets and Z+jets events. Two approaches were taken in an attempt to rectify the remaining differences. The first is a photon smearing method as used in [3]. This is done by looking at the component of the $E_{\mathrm{T}}^{\mathrm{miss}}$ along the Z/photon direction, $E_{T,||}^{\mathrm{miss}}$. The idea is that any difference in $E_{T,||}^{\mathrm{miss}}$ between Z+jets and γ+jets events comes from lepton mis-measurements in the Z+jets events, leading to a larger Z resolution compared to the photon. Hence the photon p_{T} and $E_{T,||}^{\mathrm{miss}}$ can be smeared to match the Z resolution. This procedure was carried out in the mono-Z analysis but minimal improvements were seen because the photon and Z were observed to have very similar resolutions. Therefore a second reweighting scheme was adapted to improve the agreement in the $E_{\mathrm{T}}^{\mathrm{miss}}$ distributions. Instead of only reweighting by p_{T}, a secondary reweighting is applied using another variable. Several variables were investigated; in the end E_T^{miss}/H_T gave the best results (H_T = scalar sum of lepton p_{T} and jet p_{T}). In addition, the reweighting could be applied using 2D weights or with two 1D (2x1D) weights. The 2D reweightings that were investigated gave the best $E_{\mathrm{T}}^{\mathrm{miss}}$ agreement, but the weights were unreliable due to limited statistics (e.g. weights in p_{T} and E_T^{miss}/H_T bins). 2x1D reweighting schemes were also studied. Here an added complication is that the two variables that are reweighted are treated as uncorrelated, whereas for 2D reweighting the correlation is accounted for automatically. So in a 2x1D scheme, when reweighting the second variable, if the previously reweighted p_{T} distribution does not change, then the variables can be treated uncorrelated. This was seen in p_{T} and E_T^{miss}/H_T. Also the weights with 2x1D schemes were observed to be far more reliable because of the higher statistics use in the weight calculation. This was further tested by splitting the γ+jets MC into two statistically independent halves; one half was used to obtain the weights and the other half had them applied. The agreement between both reweighted halves of the γ+jets sample was excellent.

Due to time constraints in the analysis for the 2015+2016 result, the development of this technique is still under development and has yet to be tested on data. In the end a 2x1D reweighting scheme using p_{T} and E_T^{miss}/H_T gave the best results in MC. Figure 3.4 shows the $E_{\mathrm{T}}^{\mathrm{miss}}$ distributions for Z+jets and reweighted γ+jets events (at an early selection step). From Z+jets MC, the predicted yield in the ee and $\mu\mu$ signal regions is approximately 0.45 ± 0.90

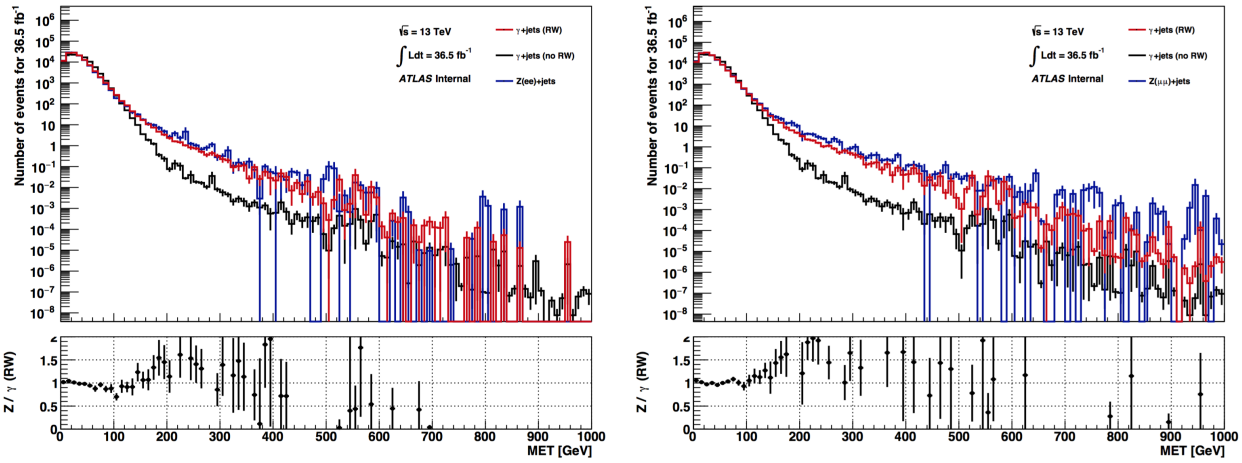

Figure 3.4: $E_{\mathrm{T}}^{\mathrm{miss}}$ distributions for γ+jets events (red) and Z+jets events (black without reweighting, blue with reweighting).

events. The best observed reweighted γ+jets prediction is 2.0 ± 0.1. The results nearly agree within statistical errors, but differences are still observed in the $E_{\mathrm{T}}^{\mathrm{miss}}$ tail. Since this is the region of interest in the mono-Z search, care must be taken to study these differences and quantify the systematic errors from the reweighting technique. The next steps to developing and improving the γ+jets technique are discussed in the next chapter.

3.4 Dark Matter Limit Setting

In the case that no excess is observed in data, upper limits are set on the signal strength for each of the dark matter models. These are then translated into limits on the masses of the dark matter particles, m_χ and m_{med}. Hypothesis tests are performed using HistFitter. The signal region $E_{\mathrm{T}}^{\mathrm{miss}}$ distributions are inputted to HistFitter for signal, backgrounds, and all systematic uncertainties (also known as nuisance parameters or NPs). HistFitter calculates upper limits using the CL_s method [4], a standard in the ATLAS experiment.

The statistical analysis of the data uses a binned likelihood function constructed as the product of Poisson probability terms,

$$\mathcal{L} = \mathrm{Pois}(n|\mu s + b) \left[\prod_{b \in \mathrm{bins}}^{n} \frac{\mu \nu_b^{\mathrm{sig}} + \nu_b^{\mathrm{bkg}}}{\mu s + b} \right], \tag{3.4}$$

where μ, the signal strength parameter, multiplies the expected signal yield ν_b^{sig} in each histogram bin b, and ν_b^{bkg} represents the background content for bin b. The dependence of

the signal and background predictions on the systematic uncertainties is described by a set of NPs $\vec{\theta}$, which are each parametrized by a Gaussian.

The nominal fit result is obtained by maximizing the likelihood function with respect to all parameters. This is referred to as the maximized log-likelihood, $\mathcal{L}(\hat{\mu}, \hat{\boldsymbol{\theta}})$, where $\hat{\mu}$ and $\hat{\boldsymbol{\theta}}$ are the parameters that maximize the likelihood. The test statistic $\tilde{q}_\mu$ is then constructed based on the profile likelihood ratio:

$$\lambda(\mu) = \frac{\mathcal{L}(\mu, \hat{\hat{\boldsymbol{\theta}}})}{\mathcal{L}(\hat{\mu}, \hat{\boldsymbol{\theta}})} \tag{3.5}$$

$\hat{\hat{\boldsymbol{\theta}}}$ are the nuisance parameter values that maximize the likelihood for a given μ. The level of compatibility is quantified using $\tilde{q}_\mu$, since larger values are interpreted as greater incompatibility between data and the assumed signal+background ($\mu = 1$) hypothesis. The corresponding p-value, p_μ, is defined as:

$$p_\mu = \int_{\tilde{q}_{\mu,\mathrm{obs}}}^{\infty} f(\tilde{q}_\mu|\mu)\mathrm{d}\tilde{q}_\mu \tag{3.6}$$

Here $f(\tilde{q}_\mu|\mu)$ is the probability density function of $\tilde{q}_\mu$ assuming the μ hypothesis, and $\tilde{q}_{\mu,\mathrm{obs}}$ is the value of $\tilde{q}_\mu$ computed for the observed data. Asymptotic formulae [4] are used to calculate the closed form for $f(\tilde{q}_\mu|\mu)$. p_μ can also be written as:

$$p_\mu \equiv p_{s+b} = P(\tilde{q}_\mu \geq \tilde{q}_{\mu,\mathrm{obs}}|s+b) \tag{3.7}$$

Performing exclusion tests with p_{s+b} is known as the CL_{s+b} method. This analysis uses the CL_s method, where the p-value, or the "CL_s value," is defined as:

$$\mathrm{CL}_s \equiv \frac{p_{s+b}}{1-p_b}, \tag{3.8}$$

where

$$p_b = P(\tilde{q}_\mu \leq \tilde{q}_{\mu,\mathrm{obs}}|b). \tag{3.9}$$

Using the CL_s method, any μ values that give $\mathrm{CL}_s < 0.05$ are excluded at the 95% confidence level (CL). These upper limits on μ are then extracted from HistFitter, and dark matter mass exclusion limits are produced using the MonoZLimitsUVic framework that was written for this purpose.

Figure 3.5 shows the exclusion limits from the 2015+2016 result on m_χ vs m_{med} for

axial-vector and vector mediators from the LO simplified models. The mass region inside the contour is excluded at the 95% CL. The relic density line indicates where the particles and interactions of the model are by themselves sufficient for explaining the observed DM abundance in the universe.

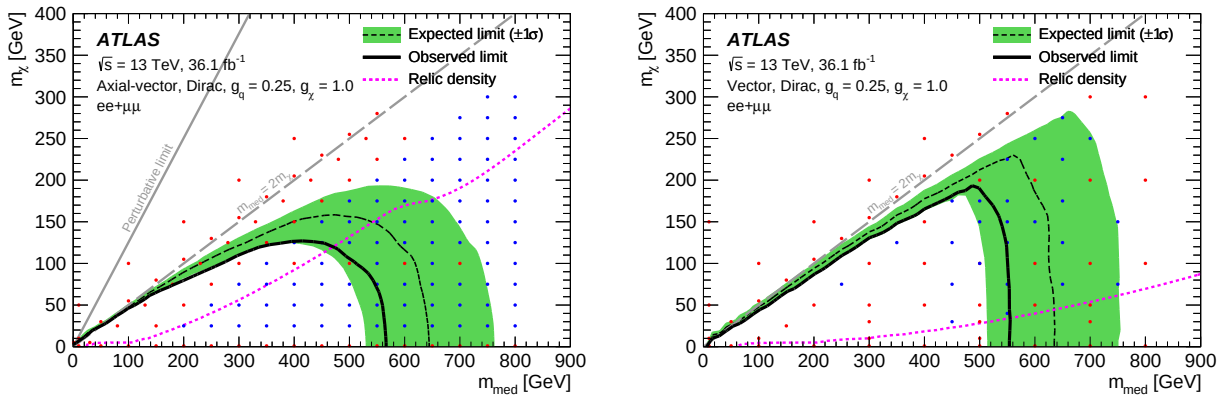

Figure 3.5: Axial-vector (a) and vector (b) exclusion limits on m_χ vs m_{med} with 36.1 fb^{-1}.

The 2D mass limits have also been recast into limits on the DM-proton scattering cross section for comparison with DD experiments. The procedure for doing so is given in [5]. Figure 3.6 shows the recast mono-Z limits for the spin-dependent (SD) and spin-independent (SI) scattering cross sections vs m_{med}. The cross section is SD if the isotope used in the DD experiment has an unpaired proton or neutron. The limits shown are at the 90% CL in accordance with the standard used by DD experiments. The coloured lines overlaid are limits set by DD experiments.

Exclusion limits on the 2HDM+PS model have also been set with the 2015+2016 dataset. These are shown in Figure 3.7. Limits are set on m_H vs m_a as well as $\tan(\beta)$ vs m_a.

In the mass limits above, the red points indicate the masses at which there are reconstructed signal samples. The blue points indicate *emulated* points. Mass point emulation is performed to create a finer grid of signal samples without using reconstructed samples. The exclusion contour may look jagged in areas with a coarse grid of signal points. By adding in emulated points, the contour can be made smoother and more physical without going through the tedious process of requesting additional reconstructed MC samples. The method discussed here has been used for the LO simplified models with 36.1 fb^{-1}; emulation for the 2HDM+PS model is more complicated and is not discussed here.

The validity of emulating signal samples relies on the assumption that the kinematics (i.e. the $E_{\text{T}}^{\text{miss}}$ distributions) of the signal does not depend on m_χ in the on-shell region

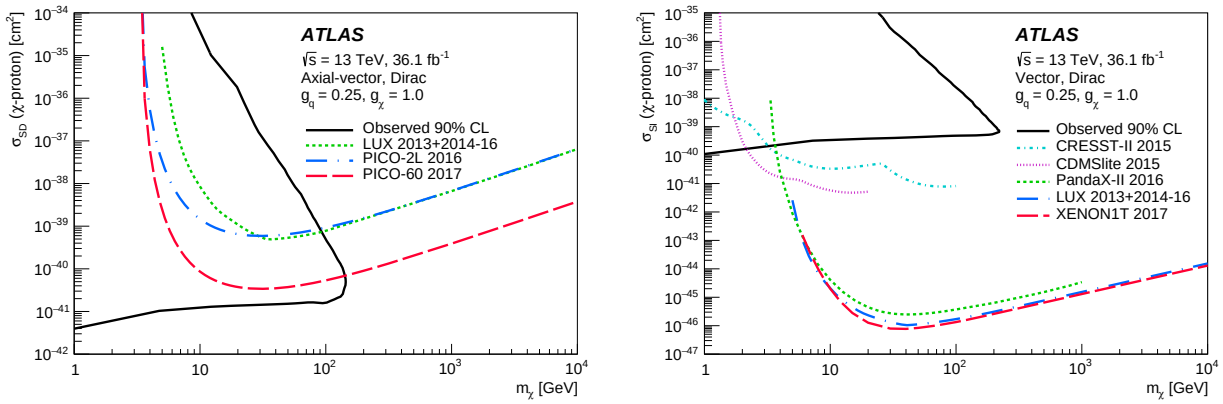

Figure 3.6: Axial-vector (a) and vector (b) exclusion limits on the DM-nucleon scattering cross section vs m_{med} with 36.1 fb^{-1}.

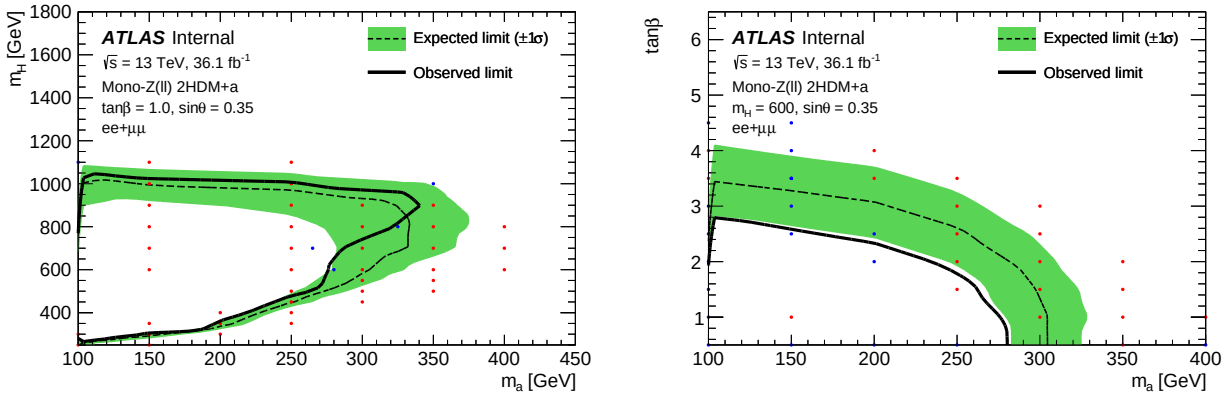

Figure 3.7: m_H vs m_a (a) and tan(β) vs m_a (b) exclusion limits with 36.1 fb^{-1}.

(where $m_{\text{med}} > 2m_\chi$). If this is true, then the E_T^{miss} distribution for a reconstructed sample at a given m_{med} can be used as the $E_{\text{T}}^{\text{miss}}$ distribution for other signal samples with the same m_{med}. However, the $E_{\text{T}}^{\text{miss}}$ distribution for the emulated sample must be scaled by the ratio of cross sections $\sigma_{\text{reco}}/\sigma_{\text{emul}}$. So, as long as the grid of reconstructed points is fine along m_{med}, additional points with different m_χ can be emulated just by using the cross sections.

For the axial-vector model, studies on the signal acceptance were been performed and verified that the signal acceptance is flat for a fixed m_{med}. For the vector model, an additional complication was that we had a fairly coarse granularity of reconstructed points along m_{med}. Because of this, we exploited the similar kinematics between the axial-vector and vector signals and performed emulation from axial-vector $\rightarrow$ vector samples. Emulation for both models has become customary in the mono-Z analysis and will continue to be used moving

forward towards the full dataset.

3.5 Analysis Software

The MonoZUVic software package is the core of the analysis and has been developed by the UVic group for the past few years. Throughout the evolution of the analysis, contributions have been made towards writing and maintaining the software. The software must be capable of running the entire analysis, including object (electron, muon, jet) calibrations/corrections/selections, removal of overlaps between objects, applying event selections, calculating event weights and kinematic variables, evaluating experimental systematics, and in the end producing trees/histograms for data and MC. Things like calibration recommendations and data formats are in flux quite frequently, and diligent efforts are made to keep the code updated. The software is also cross checked with other groups running the analysis to ensure updated calibrations, squash bugs, etc. The MonoZTruthUVic and MonoZLimitsUVic packages, mentioned briefly above, were written to perform truth-level studies and produce exclusion limits. These packages are also be maintained alongside MonoZUVic. Contributions have also been made to design overhauls in the framework as the analysis has evolved and improved.

Chapter 4

Analysis with the Full Run 2 Dataset

4.1 Event Selection Optimization

For the full Run 2 analysis the event selection for the signal region will need to be reoptimized. In practice this is done by defining multiple potential signal regions with each cut varied in intervals (e.g. $E_{\mathrm{T}}^{\mathrm{miss}} > 80$, 85, 90, 95, 100, ... GeV). Then in each region the signal significance Z is calculated. The formula used in the past iterations of the analysis is given by [6]:

$$Z = \sqrt{2\left((s+b)\ln\left(1+\frac{s}{b}\right)-s\right)} \tag{4.1}$$

s and b are the expected number of signal and background events in MC, and $s+b$ follows a Poisson distribution. If $s \ll b$ then the formula reduces to $Z = s/\sqrt{b}$. The main caveat with this formula however is that the uncertainty on b is considered to be negligible. If one takes the uncertainty on b to be σ_b, then the formula becomes:

$$Z = \sqrt{2\left((s+b)\ln\left(\frac{(s+b)(b+\sigma_b^2)}{b^2+(s+b)\sigma_b^2}\right)-\frac{b^2}{\sigma_b^2}\ln\left(1+\frac{\sigma_b^2 s}{b(b+\sigma_b^2)}\right)\right)} \tag{4.2}$$

This formula reduces to $Z = s/\sqrt{b+\sigma_b^2}$ for $s \ll b$ and $\sigma_b^2 \ll b$. Using this formula would be an improvement compared to using Equation 4.1. The significance is estimated from MC, so the uncertainties σ_b could be either (a) the experimental systematics as applied to the MC, or possibly (b) approximated from the much larger data-driven uncertainties on the background estimates from the 2015+2016 result. These uncertainties were calculated in a specific signal region, but their approximate magnitudes could be useful for estimating a more conservative significance.

A reoptimization of the signal region is also motivated by newly available $E_{\mathrm{T}}^{\mathrm{miss}}$-related quantities that could improve the mono-Z analysis. For example, two $E_{\mathrm{T}}^{\mathrm{miss}}$ working points are now available. In the new "tight" $E_{\mathrm{T}}^{\mathrm{miss}}$ definition, jets in the forward region of the detector must have $p_{\mathrm{T}} > 30$ GeV to reduce contributions from pileup. The "loose" definition (used previously in this analysis) includes all jets with $p_{\mathrm{T}} > 20$ GeV except for forward jets with $p_{\mathrm{T}} < 60$ GeV that fail an additional minimum jet vertex tagger (JVT) requirement, a multivariate criteria that identifies pileup jets from tracks. The tight definition is now recommended because the $E_{\mathrm{T}}^{\mathrm{miss}}$ resolution is improved. Both definitions will be studied to validate the improvement in switching to the tight definition.

Another new variable is the $E_{\mathrm{T}}^{\mathrm{miss}}$ significance $\mathcal{S}$. It is defined using a log-likelihood ratio to estimate how likely it is that the reconstructed $\vec{E}_{\mathrm{T}}^{\mathrm{miss}}$, summed from all reconstructed objects, is consistent with the true $\vec{E}_{\mathrm{T}}^{\mathrm{miss}}$ according to:

$$\mathcal{S} = 2 \ln \left(\frac{\mathcal{L}(\vec{E}_{\mathrm{T}}^{\mathrm{miss}} = \sum_i \vec{E}_{\mathrm{T},i}^{\mathrm{miss}})}{\mathcal{L}(\vec{E}_{\mathrm{T,true}}^{\mathrm{miss}} = 0)} \right) \tag{4.3}$$

In other words, the significance measures how well the measured $\vec{E}_{\mathrm{T}}^{\mathrm{miss}}$ agrees with the null hypothesis that $\vec{E}_{\mathrm{T,true}}^{\mathrm{miss}} = 0$, i.e. there really is no $E_{\mathrm{T}}^{\mathrm{miss}}$ in the event. This discriminant is more powerful in rejecting events with fake $E_{\mathrm{T}}^{\mathrm{miss}}$ from mis-measured objects (compared to more traditional variables such as E_T^{miss}/H_T) because it includes the uncertainties of the reconstructed objects and track-based soft term that enter the $E_{\mathrm{T}}^{\mathrm{miss}}$ calculation. Hence this is a promising variable to help reduce the Z+jets background, arguably the most difficult background to estimate in this analysis.

Finally, an added complication in the future event selection optimization of the analysis is the potential for multiple signal regions. As we study more varieties of dark matter models, the cuts that optimize the significance for different signals may change. If the significance for different signals varies greatly with different cuts, it may be optimal to have more than one signal region. However, this adds additional challenges to the analysis, such as having to estimate backgrounds in multiple regions; if a background is difficult to estimate (e.g. large correlations when estimating Z+jets with the ABCD method), this can increase the amount of time needed to validate the technique and obtain a reasonable data-driven estimate. Since the analysis has limited manpower, it may be decided to have a slightly sub-optimal signal region and sacrifice some significance. These types of decisions will have to be discussed in the group moving forward.

4.2 Development of the γ+jets Technique

The γ+jets method for estimating the Z+jets background is under development. For the 2015+2016 result, a heavily modified ABCD method was used for the Z+jets data-driven estimate. The systematic errors on the estimate were large, on the order of 50-100%. It would be ideal to have a more reliable estimate for this background from the γ+jets method for the full Run 2 result.

As discussed in Section 3.3.2, for the 2015+2016 result acceptable agreement was seen between MC γ+jets and Z+jets events in the signal region, with the estimates nearly agreeing within statistical errors. The method used a 2x1D reweighting scheme with the boson p_{T} and the E_T^{miss}/H_T. After the reoptimization of the event selection, this scheme may change. For example, with the introduction of the $E_{\mathrm{T}}^{\mathrm{miss}}$ significance described in the previous section, it may be ideal to redo the γ+jets estimate with p_{T} and $\mathcal{S}$, that is if $\mathcal{S}$ is chosen to be included in the event selection. Depending on the selections chosen, it could be worth reinvestigating a few of the more promising pairs of variables to perform the reweighting with. In addition, the improved statistics of the Run 2 dataset may provide opportunity for more reliable 2D weights, but this will need to be assessed. It may also be worthwhile to investigate the effects of the reweighting before/after certain cuts. For example, the largest disagreement between γ+jets and Z+jets events in the cutflow was seen at the $E_{\mathrm{T}}^{\mathrm{miss}}$ (and E_T^{miss}/H_T) cut. It could be that reweighting the events after the $E_{\mathrm{T}}^{\mathrm{miss}}$ requirement may help to improve the agreement.

Once acceptable agreement is seen in γ+jets and Z+jets events, the next step would be to apply the method to data. A few methods for doing this have been discussed. For example, should the weights be obtained from data or MC? This may depend on which has more reliable statistics. The validation of the weights must also be tested, for example by applying weights obtained in MC to data and then looking at the agreement with the reweighted MC. Differences seen in the agreement must then be quantified as systematic errors in the technique.

There is also the technical side of implementing the γ+jets technique in the MonoZUVic software. This was done previously for the 2015+2016 result, but since then the code has undergone a significant redesign, and the γ+jets estimate will need to be reimplemented.

4.3 Signal Models

More dark matter models with be studied in the mono-Z analysis with the full Run 2 dataset. As recommended by the LHC DM Working Group, s-channel simplified models with spin-0 mediators will continue to be the benchmark model used in the analysis; however signals will be simulated at NLO in QCD rather than LO, as higher-order QCD corrections have been shown to have a significant impact on the production rate and kinematic distributions of these models [7]. In addition, these models allow for mediator couplings to leptons. In total there are four NLO benchmark scenarios recommended [8] with the following couplings:

Model	Mediator	g_q	g_ℓ	g_χ
A1	axial-vector	0.25	0.0	1.0
A2	axial-vector	0.1	0.1	1.0
V1	vector	0.25	0.0	1.0
V2	vector	0.1	0.01	1.0

Table 4.1: Benchmarks for NLO s-channel simplified models in Run 2.

Chris Anelli has recently done work to show that it is possible to rescale from A1→A2 and V1→V2 using the ratio of cross sections. We are currently working on sample requests for the A1 and V1 models, and scaling will be done for the A2 and V2 scenarios. Mass point emulation will also be carried out again to reduce the number of reconstructed samples needed. The full Run 2 dataset is expected to be ∼140 fb^{-1}. To estimate how the limits will improve for such a dataset, the NLO limits obtained with 36.1 fb^{-1} have been scaled to an integrated luminosity of 140 fb^{-1}. Figure 4.1 shows a projection from Chris for the NLO vector limits. This projection assumes the same signal region and background estimates as used for the 2015+2016 result. These will of course change with the full dataset, but it gives an estimate for the masses at which we should request samples. Compared to 36.1 fb^{-1}, the expected reach in m_{med} improves from 550 GeV to nearly 900 GeV for light m_χ, and the maximum reach in m_χ improves from 250 GeV up to 350 GeV.

In addition to the simplified models, the 2HDM+PS model has become a new standard in the analysis. A similar projection to 140 fb^{-1} will be done using the limits on m_H vs m_a and $\tan\beta$ vs m_a with 36.1 fb^{-1} shown in Section 3.4, and a request for more reconstructed samples will follow suit. Mass point emulation for the 2HDM+PS model is more complicated than for the simplified models; both the signal acceptance and the $E_{\mathrm{T}}^{\mathrm{miss}}$ shape depend non-trivially on m_a and m_H, and the best method for emulating samples is still being investigated.

The other type of signature to be investigated with the full Run 2 dataset is the t-channel

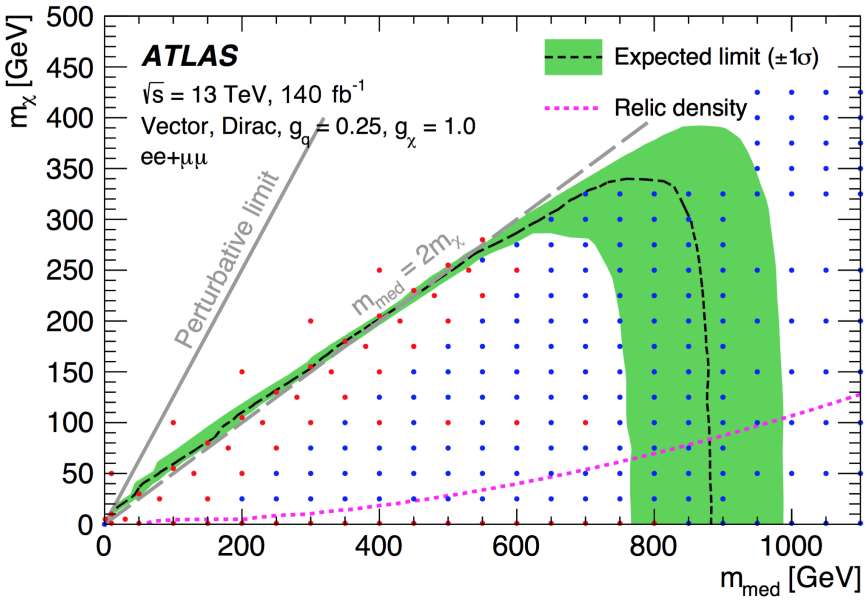

Figure 4.1: Prospective NLO s-channel vector exclusion limit with 140 fb^{-1}. Produced by Chris Anelli.

signature with a coloured scalar mediator. There are various models that encompass this type of signature (Figure 4.2 shows the relevant t-channel diagrams for mono-Z). A few potential models to be considered are discussed here. These models are of interest for the mono-Z search because the Z is allowed to couple directly to the mediator, a channel unique to mono-Z.

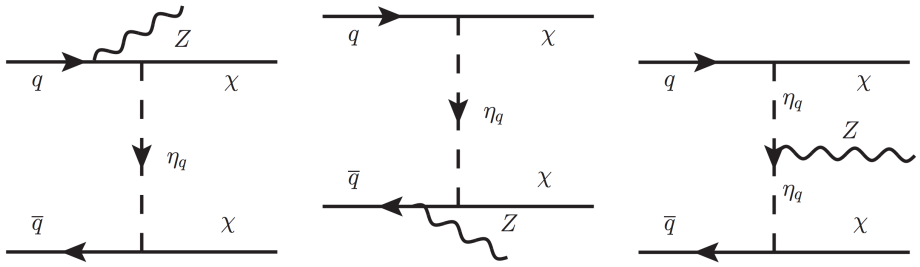

Figure 4.2: t-channel diagrams with the mono-Z signature.

The Papucci model [9] was the first t-channel model recommended by the LHC DM WG in [10]. The interaction Lagrangian is given by:

$$\mathcal{L}_{\text{int}} = g \sum_{i=1,2} \left(\eta_{(i),L} \bar{Q}_{(i),L} + \eta_{(i),u,R} \bar{u}_{(i),R} + \eta_{(i),d,R} \bar{d}_{(i),R} \right) \chi \tag{4.4}$$

Here $Q_{(i),L}$, $u_{(i),R}$, and $d_{(i),R}$ are the SM quarks, $\eta_{(i),L}$, $\eta_{(i),u,R}$, and $\eta_{(i),d,R}$ are the mediator particles, and g is the coupling between the SM particles and dark matter. L and R indicate left- and right-handedness, and the index i is the quark generation. In the Papucci model only the first two generations are considered.

The mono-jet analysis recently set limits on the t-channel signature using the Bell model [11], a subset of the Papucci model with the interaction Lagrangian:

$$\mathcal{L}_{\text{int}} = g \sum_{i=1,2,3} \eta_{(i),L} \bar{Q}_{(i),L} \chi \tag{4.5}$$

In this model, couplings to right-handed quarks are turned off, but the third generation of quarks is included. The mono-jet analysis chose to use this model without including the third generation. This decision was based on the availability of Bell et al. to answer technical questions about the implementation/generation in MadGraph. The best choice to use for mono-Z will need to be investigated.

* TODO: less simplified models

A more complete

And there are even more models [12] currently being discussed as new benchmarks.

The mono-Z analysis currently has eight Papucci model signal samples that were requested at the start of Run 2. Hypothesis tests were run on them with 36.1 fb^{-1} of data, but none of the samples were excluded. The mono-jet analysis recently set t-channel exclusion limits using the Bell model, and their axial-vector and coloured scalar mediators exclusion regions were quite similar. Hence it was unexpected that none of the mono-Z signals were excluded. This led to some investigations, and it turns out that the mono-Z samples were generated with an incorrect mediator width. The plan now is to use MadGraph to generate t-channel samples with the correct and incorrect mediators to understand the effect on signal. If only the cross section is affected and not the $E_{\text{T}}^{\text{miss}}$, then it may be possible to scale the incorrect reconstructed samples to the correct normalization and then rerun the limit setting. From the mono-jet analysis we expect to get similar reach in mass as for the axial-vector model. Then an estimate can be made on how far the limit will reach and a full set of t-channel samples can be requested. Mass point emulation will also need to be investigated at the same time to determine how fine/coarse the grid of reconstructed points should be.

4.4 Other Analysis Improvements

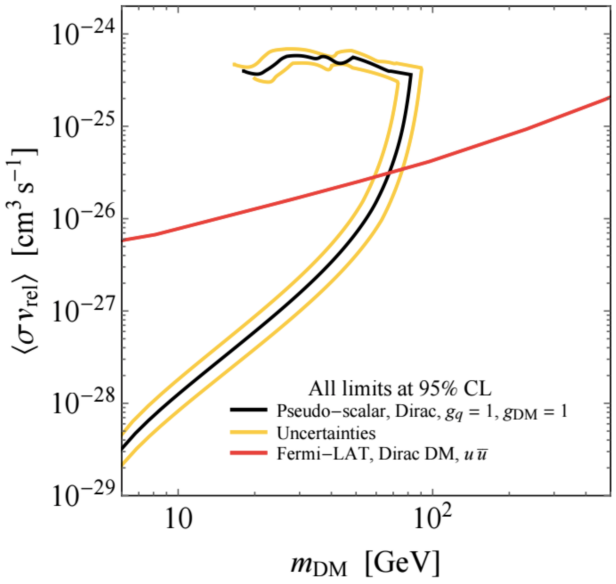

Figure 4.3: A schematic of a collider limit on $\langle \sigma v_{\rm rel} \rangle$ vs m_χ overlaid with a ID measurement [5].

The mono-Z limits have been recast into limits on the DM-proton scattering cross section for comparison with DD experiments. The same should be done to put limits on the velocity-averaged dark matter annihilation cross section into $q\bar{q}$ and compare with ID experiments. The procedure for converting the 2D mass limits into a limit on $\langle \sigma v_{\rm rel} \rangle$ is covered in [5]. Figure 4.3 gives a schematic example of what the comparison may look like.

Another improvement on the horizon for the analysis is the inclusion of weights in the signal MC generation to allow the calculation of QCD, PDF, and PS systematic uncertainties.

Finally, the analysis software...

Chapter 5

Conclusions

Appendix A

Appendix

A.1 Event Selections

A.2 Calibration Studies on Close-By Jets

Bibliography

[1] Martin Bauer, Ulrich Haisch, and Felix Kahlhoefer. Simplified dark matter models with two Higgs doublets: I. Pseudoscalar mediators. *JHEP*, 05:138, 2017.

[2] S. Ask, M. A. Parker, T. Sandoval, M. E. Shea, and W. J. Stirling. Using gamma+jets Production to Calibrate the Standard Model Z(nunu)+jets Background to New Physics Processes at the LHC. *JHEP*, 10:058, 2011.

[3] Gorm Aske Gram Krohn Galster, Tova Ray Holmes, Benjamin Henry Hooberman, Emma Sian Kuwertz, Lawrence Lee, Jonathan David Long, Zach Marshall, Judita Mamuzic, Robert McPherson, Vasiliki A. Mitsou, Christian Ohm, Ruth Pottgen, Andreas Redelbach, Giulia Ripellino, Ruo-yu Shang, Matt Zhang, Dai Kobayashi, Kerim Suruliz, Christopher John Young, and Claudia Merlassino. Another Search for strongly produced supersymmetric particles in final states containing a same-flavour opposite-sign dilepton pair, jets and missing transverse momentum in 13 TeV *pp* collisions. Technical Report ATL-COM-PHYS-2016-504, CERN, Geneva, May 2016.

[4] Glen Cowan, Kyle Cranmer, Eilam Gross, and Ofer Vitells. Asymptotic formulae for likelihood-based tests of new physics. *Eur. Phys. J.*, C71:1554, 2011. [Erratum: Eur. Phys. J.C73,2501(2013)].

[5] Giorgio Busoni et al. Recommendations on presenting LHC searches for missing transverse energy signals using simplified *s*-channel models of dark matter. 2016.

[6] Glen Cowan. 02 2018.

[7] Mihailo Backović, Michael Krämer, Fabio Maltoni, Antony Martini, Kentarou Mawatari, and Mathieu Pellen. Higher-order QCD predictions for dark matter production at the LHC in simplified models with s-channel mediators. *Eur. Phys. J.*, C75(10):482, 2015.

[8] Andreas Albert et al. Recommendations of the LHC Dark Matter Working Group: Comparing LHC searches for heavy mediators of dark matter production in visible and invisible decay channels. 2017.

[9] Michele Papucci, Alessandro Vichi, and Kathryn M. Zurek. Monojet versus the rest of the world I: t-channel models. *JHEP*, 11:024, 2014.

[10] Daniel Abercrombie et al. Dark Matter Benchmark Models for Early LHC Run-2 Searches: Report of the ATLAS/CMS Dark Matter Forum. 2015.

[11] Nicole F. Bell, James B. Dent, Ahmad J. Galea, Thomas D. Jacques, Lawrence M. Krauss, and Thomas J. Weiler. Searching for Dark Matter at the LHC with a Mono-Z. *Phys. Rev.*, D86:096011, 2012.

[12] Martin Bauer, Martin Klassen, and Valentin Tenorth. Universal Properties of Pseudoscalar Mediators. 2017.